SPARC-GE-05/001

20 June 2005

CONTRIBUTIONS TO ERL 2005

(18-23 March 2005, JLAB, USA)

1) Optimization and beam dynamics of a superconducting RF gun

2) Emittance compensation with dynamically optimized photoelectron beam profiles

OPTIMIZATION AND BEAM DYNAMICS OF A SUPERCONDUCTING RF GUN

M. Ferrario*, W. D. Moeller#, J. B. Rosenzweig+,

J. Sekutowicz#, G. Travish+

* INFN /LNF, # *DESY*, + *UCLA*

Corresponding author: M. Ferrario

INFN-LNF

Via E. Fermi 40

00044 Frascati (Roma), Italy

Phone: ++39-06-94032216

FAX: ++39-06-94032565

e-mail: Massimo.ferrario@lnf.infn.it

ABSTRACT

Recent advances in superconducting rf technology, and an better understanding of rf the photoinjector design optimization make it possible to propose a specific design for a superconducting rf gun which can simultaneously produce both ultra-high peak brightness, and high average current. Such a device is a critical component of next generation x-ray sources, such as self-amplified spontaneous emission free-electron lasers (SASE FEL) and energy recovery linac (ERL) based systems. The design presented in this paper is scaled from the present state-of-the-art normal conducting rf photoinjector that has been studied in the context of the LCLS and SPARC SASE FEL injection schemes. Issues specific to the superconducing rf photoinjector, such as accelerating gradient limit, rf cavity and cryostat design, and compatibility with magnetic focusing and laser excitation of a photocathode, are discussed.

PACS: 41.60.Cr

Keywords: : High Brightness Beams, Superconducting Injector, Energy Recovery Linac

1. INTRODUCTION

With the advent of existing [1] and proposed [2,3] superconducting radio-frequency (SRF) electron linear accelerators dedicated to radiation production and high energy physics, the demands on the sources that supply electrons to these devices are increasing. These demands run in two somewhat opposing directions: i) the quality of each beam bunch must be very high, as measured by the peak brightness, the ratio of the peak beam current to the transverse phase space volume, $B = 2I_p / \epsilon_n^2$, and ii) the duty factor and average beam current should be as high as possible, to take full advantage of SRF-specific capabilities. As a rule, to enhance brightness one has to expose the photo-emitting cathode to a very high electric field, and also to introduce magnetic solenoid fields within the photoinjector gun region. These focusing fields allow for control and mitigation of space-charge effects, a process termed emittance compensation [4].

The demand for high duty factor logically pushes one to consider the possibility of using a SRF photoinjector gun. In fact for some proposed sources [3], one would like to run the entire system, linac and injector, in continuous-wave (CW) mode, a operational mode which presents extreme challenges for a normal conducting RF gun.

In previous examinations of the likely implementation of a photocathode SRF gun [5] it was assumed that one needs to provide significant focusing inside of the gun, near the cathode. This assumption has been partially driven by the initial relatively low estimate of the available field gradient [6]. A solution to provision of transverse beam control near the cathode has been proposed which uses so-called “RF focusing” [7], which requires a deformation of the cathode plane. Unfortunately, this technique provides insufficient focusing for a full control of emittance oscillations, and in addition the back wall deformation introduces nonlinear field components that may also cause significant emittance growth in the injector.

Some experimental efforts have been made recently to investigate the feasibility of a SRF photocathode gun [8,9]. Various proposals have been made to address the photo-cathode issue, including the direct use of the superconducting Nb material [10], the deposition of a thin layer of higher quantum efficiency material on the Nb substrate [11], and the introduction of a non-superconducting cathode that is thermally isolated from the rest of the SRF cavity [12]. It is crucial that a relatively high quantum efficiency (η) be obtained from the photocathode, in order to lower the needed drive laser flux impinging on the cavity. The limit

on flux comes from source considerations — what a reasonable technical configuration of the laser system may be — or from concerns about the thermal load on the superconducting surfaces [13].

It will be shown in this paper that a highly optimized design of an SRF photocathode gun may be now considered by simple scaling of existing high brightness sources to lower RF frequency. In the proposed 1.3 GHz configuration, the peak accelerating gradient in the gun cavity is seen to be within that demonstrated by the TESLA program at the same frequency [14]. Further, this scaled configuration adopts a focusing solenoid geometry that keeps nearly all of the magnetic field strength outside of the cavity. The magnetic field in fact must not penetrate the super-conducting cavity, in order to avoid thermal break-down when the critical field of 200 mG is exceeded, and to avoid any residual flux trapping that may cause cavity Q_0 degradation.

An experimental program is now under way at DESY and BNL in order to investigate quantum efficiency properties of lead, that is also a superconducting material. Preliminary results show that a quantum efficiency of the order of 1.5 x 10^{-3} can be obtained from a Pb photocathode illuminated by a 213 nm laser pulse [11]. If these results are confirmed, a 1 nC, 1 MHz repetition rate beam (1 mA average current) could be generated by a 4 W pulsed laser soruce. The needed high repetition rate, high average power UV laser can be conventionally produced from a set of commercially available Ti:Sapphire regenerative amplifiers (for instance, the Coherent RegA at 250 KHz and about 1.2 W average power), combined to produce the repetition rate and frequency quadrupled. Alternatively, recent advanced in fiber lasers [15] may soon provide the necessary pulse format and power at around 1 or 1.5 μm where a sum-frequency mixing scheme can produce the UV [16]. The former approach is available today but is expensive, whereas the later approach is still a year or two from being practical but can take advantage of extensive development work being done for UV lithography (mostly at 193 nm). With such a cathode/laser system the design of the SRF gun will be highly simplified. The drawback of this approach is thermal emittance that increases with the photon energy [17] but a convenient beam parameter set can be found in order to keep the thermal emittance below the 1 μm threshold.

The extreme case of ampere class superconducting guns is discussed in Ref. [18]. These devices require careful control of the higher order mode trapping and are specifically designed with wide beam tubes to facilitate damping of unwanted trapped HOM. The

adoption of an external, optimized solenoid will certainly provide additional benefit for producing ultra-high brightness beams also for these high average current class guns.

Another proposed scheme is to excite a TE magnetic mode inside the cavity which focuses the electron beam and prevents the increase of the transverse emittance [19]. The HOM magnetic mode is unfortunately not a harmonic of the accelerating mode. This results in phase-dependent behaviour in the focusing, and thus in the emittance compensation process.

2. BASIC DESIGN APPROACH

In a space charge dominated beam, *i.e.* when the space charge collective force is largely dominant over the emittance pressure, the induced emittance growth in an RF gun is highly correlated. These can be reduced by a simple focusing scheme [4]. A full theoretical description of the emittance compensation process [20] has demonstrated that in this regime mismatch between the space charge correlated forces and the external focusing gradient produces slice envelope oscillations (or equivalently, transverse plasma oscillations) that in turn produce normalized emittance oscillations downstream the gun cavity. It has also been shown that to damp these emittance oscillations the beam must be matched properly at injection into an accelerating section to the so-called invariant envelope. This matching should be maintained until the space charge forces are diminished by acceleration.

Following the previous matching condition a new working point suitable to damp emittance oscillations has been recently found [21, 22] in the context of the LCLS FEL project [23]. This working point can be easily scaled [24] to any other frequency, gradient [22] or charge design. In addition, in this configuration the location of the solenoid field can be shifted towards the gun cavity exit, resulting in an excellent condition for a high brightness superconducting RF gun.

The design for the LCLS photoinjector utilizes the peak electric field on-axis between 120 and 140 MV/m at an operating rf frequency of 2.856 GHz [23]. While such fields clearly exceed those achievable in superconducting rf cavities, one may easily scale the fields downward by moving to a different design frequency [24]. As the longitudinal beam dynamics are preserved in this case by scaling the fields as $E_0 \mu \nu_{rf}^{-1}$, at L-band (1.3 GHz) the needed peak on-axis field is between 54 and 64 MV/m, which is roughly equivalent to an average accelerating field between 27 and 32 MV/m. These fields are the state-of-the-art

superconducting cavities technology [14]. The working point of the LCLS photoinjector is predicted to have a very high brightness, with a peak current at 1 nC charge of 100 A (10 psec flat-top pulse), and an emittance of 0.6 μm [23]. With these beam parameters, obtained from detailed PARMELA simulation, the brightness is calculated to be B = 5.6 x 10^{14} A/m^2.

One may scale the space-charge dominated beam dynamics naturally and exactly in rf wavelength, by scaling the beam dimensions by the rf wavelength $\lambda_i \sim \lambda_{rf}$ the solenoid field as $B_z \sim \lambda_{rf}^{-1}$, and the beam charge by $Q \sim \lambda_{rf}$ [24]. Under these assumptions, the current is independent of λ_{rf}, and the emittance scales as λ_{rf} - thus the brightness $B \sim \lambda_{rf}^{-2}$. Fortunately, if we scale back the charge at L-band from 2.2 nC (natural scaling), to 1 nC, we do not pay such as strong (factor of five) penalty in brightness.

For charge scaling, we must keep the beam plasma frequency constant, which dictates that $\lambda_i \sim Q^{1/3}$. Under the conditions of both charge and wavelength scaling, it can be shown that the emittance scales [24] as

$$\varepsilon_n(\mu m) = \lambda_{rf}(m)\sqrt{a_1\left(\frac{Q(nC)}{\lambda_{rf}(m)}\right)^{2/3} + a_2\left(\frac{Q(nC)}{\lambda_{rf}(m)}\right)^{4/3} + a_3\left(\frac{Q(nC)}{\lambda_{rf}(m)}\right)^{8/3}}$$

where the constants a_i are deduced from simulation scans. These constants have physical significance: a_1 measures the contribution of thermal emittance; a_2 the component due to space charge; a_3 the emittance arising from rf and chromatic effects. For the LCLS designs "family" , these constants are determined to be: $a_1 = 1.5$, $a_2 = 0.81$, $a_3 = 0.052$

The current can likewise scaled as:

$$I(A) = a_4\left(Q(nC)/\lambda(m)\right)^{2/3}$$

($a_4 = 22.5$) to yield a brightness scaling of:

$$B\left(A/m^2\right) = \frac{2\cdot 10^{12}}{a_1\lambda_{rf}^2(m) + a_2 Q^{4/3}(nC)\lambda_{rf}^{2/3}(m) + a_3 Q^2(nC)}$$

which has an interesting limit for very small charges (due to thermal effects):

$$B_{max}\left(A/m^2\right) = \frac{3\cdot 10^{13}}{\lambda_{rf}^2(m)}$$

For our L-band scaled design at 1 nC charge, we obtain a current of 60 A, and an emittance, as before, of 0.6 μm, for a peak brightness of B = 3.2 x 10^{14} A/m^2 which we expect from a potentially very high brightness *superconducting* source. The possibility is thus within reach that a scaled SRF version of the LCLS injector may give bunches of electrons with extremely high brightness, at average repetition rates well in excess of the present state of the art.

3. SRF CAVITY AND SOLENOID DESIGN

A simple and attractive approach to cavity/cathode design has been proposed at BNL [10]. The basic idea is to illuminate the back wall of the superconducting Nb cavity with UV laser, obtaining photo-emission and the electromagnetic cavity from a single integral structure. This strategy guides our cavity design as well. The proposed 1.3 GHz 1.6 cell Nb cavity, used here as a basis for studying beam dynamics in the injector, is shown in Fig. 1.

The design of the cell shape was guided by the same considerations adopted by the TESLA cavities: i) a spherical contour near the equator with low sensitivity to multipacting, ii) minimization of electric and magnetic fields at the cavity wall to reduce the danger of field emission and thermal breakdown, and iii) a large iris radius to reduce wake field effects. The full cell dimensions are the same of a inner cell of a TESLA cavity, while the first is longer than a half cell ($0.6\lambda_{rf}/4$) in order to compensate for phase slippage occurring at the beginning of the non relativistic beam acceleration. A coaxial input power coupler has been adopted, as in the normal conducting TESLA gun design, in order to prevent any asymmetry in the accelerating field and thus to diminish transverse RF kicks. The HOM coupler is placed on the beam tube close to last cell iris [25].

In Fig. 1, a schematic design of the gun/solenoid system is shown, including also the μ-metal box around the cavity already foreseen to screen the Earth magnetic field. With 1 mm thick μ-metal the residual magnetic field on the last iris surface is reduced to only 20 mG. a value that could be further reduced by increasing the screen thickness. At this level the residual fringe field is tolerable, in that the focusing field is applied only after cool down and the small field that would nominally enter the superconducting cavity is excluded by the Meissner effect. The scheme shown in Fig. 1 shows a location of the solenoid center 500 mm from the cathode. Beam dynamics simulation show that the best location for the solenoid is 360 mm from the cathode. Additional study is under way in order to find a technical solution for placing the solenoid location inside the cryostat, including the possibility of using a superconducting solenoid.

4. BEAM DYNAMICS SIMULATIONS

PARMELA simulations performed with 50,000 macro-particles are shown in Fig. 2 up to the 1 μm emittance threshold. According to the scaling approach discussed in the previous section, in our simulation we consider a uniform density 1 nC bunch, 19.8 ps long with a radius of 1.69 mm, accelerated in the gun cavity up to an energy of 6.5 MeV, corresponding to a peak field on the cathode of 60 MV/m and an injection phase of 44.5 deg. Space charge induced beam expansion (up to σ_x=2.4 mm) and emittance growth in the gun are compensated in a downstream drift with a solenoid located at the gun exit, 36 cm from the cathode, producing a 3 kG maximum field on the axis.

As shown in Fig. 2 the emittance compensation process is clearly visible in the drift until the bunch is injected at z=3.3 m in a cryomodule housing 8 L-band superconducting cavities of the TESLA type. Matching conditions for optimum emittance compensation sets the accelerating gradient to 13 MV/m. At the exit of the first cryomodule (z=14 m) the bunch has been accelerated up to 117 MeV (the beam is space charge dominated up to 90 MeV) and space charge induced emittance oscillations are totally damped [26]. The final emittance is lower than 1 μm (with a thermal emittance contribution of 0.5 μm). A minor bunch elongation in the drift results in a final peak current of 50 A. The total length of the injector system is 14 m.

A metallic photocathode increases its quantum efficiency when illuminated by a higher energy photon beam. Unfortunately also the thermal emittance ε_h of the emitted electron beam increases [17]. A Lead photocathode (work function 4.25 eV) illuminated by a 213 nm (5.82 eV) laser light has a very attractive quantum efficiency of the order of 10^{-3} that would simplify the laser system and would reduce the heat load on the cathode surface, on the other hand it would result a thermal emittance ε_h contribution of 0.7 μm/mm [17]. According to the linear scaling of thermal emittance with the laser spot size on the cathode r_b, with r_b = 1.69 mm one has ε_h= 1.1 μm. It might be convenient to rescale the beam parameters in order to reduce the thermal emittance contribution, that is the main limitation in this design, to 0.7 μm. A r_b = 1 mm laser spot size would satisfy such a request. Keeping unchanged all the other parameters including the laser pulse length (σ_t =19.8 ps) one should scale the charge according with $Q \sim r_b^2$ resulting in a 0.35 nC beam. Simulations performed by HOMDYN , see Fig. 3, show that a final emittance of 0.76 μm can be obtained with a reduced peak current of 18 A. Nevertheless with this scaling choice the beam peak brightness $B \mu \frac{Q}{\varepsilon_n^2 \sigma_t} \mu \frac{r_b^2}{r_b^2 \sigma_t}$ remains approximately unchanged.

5. ACKNOWLEDGEMENT

This work has been partially supported by the EU Commission in the sixth framework programme, contract no. 011935 – EUROFEL-DS5.

FIGURE CAPTIONS

Figure 1 . Superconducting RF gun with coaxial input coupler and SC cathode, inside of cryostat assembly.

Figure 2. Rms normalized emittance evolution in SC photoinjector, from PARMELA simulations

Figure 3. Rms normalized emittance [μm] (blue line) and beam envelope [mm] (red line) evolution along the SC photoinjector with reduced charge (0.35 nC) parameters, HOMDYN simulations

REFERENCES

[1] L. Merminga, “Technical approaches for high-average-power free-electron lasers”, Rev. Modern Phys., **74**, (2002)

[2] TESLA XFEL, Technical Design Report (Supplement), DESY 2002-167, TESLA-FEL 2002-09, (2002).

[3] J. Sekutowicz et al., “Proposed Continuous Wave Energy Recovery Operation of an XFEL”, Phys. Rev. ST-AB, **8**, 010701 (2005).

[4] B. E. Carlsten, Nucl. Instrum. Methods A **285**, 313 (1989).

[5] H. Piel, et al., Proceedings of the 10th FEL Conference, Jerusalem, 1998.

[6] C. Pagani, P. Michelato, L. Sera"ni, Nucl. Instr. and Meth. A 340 (1994) 17.

[7] D. Janssen, V. Volkov, Nucl. Instr. and Meth. A 452 (2000), 34.

[8] D. Janssen et al., , Nucl. Instr. and Meth. A 507 (2003), 314.

[9] A. Michalke, Internal report, WUB-DIS 92–5, Universitat Wuppertal 1993.

[10] T. Srinivasan-Rao et al., “Design, Construction and Status of All Niobium Superconducting Photoinjector at BNL”, PAC03, Portland 2003, USA

[11] J. Smedley et al.,Progress on Lead Photocathodes for Superconducting Injectors, Proc of PAC 2005, Knoxville, Tennessee, USA

[12] X. Chang et a., Study of Secondary Emission Enhanced Photoinjector , Proc of PAC 2005, Knoxville, Tennessee

[13] T. Schultheiss et al., “Thermal/Structural analysis of a SCRF Photocathode Electron Gun Cavity”, PAC01, Chicago 2001, USA.

[14] L. Lilje, “Achievement of 35 MV/m in the TESLA Superconducting Cavities Using Electropolishing as a Surface Treatment”, Proc. of EPAC 2004, Lucerne, Switzerland

[15] A. Malinowski, *et al.*, Optics Letters, V29, No17, 2073-2075 (2004).

[16] I.Z. Kozma, *et al.,* Opt. Express **11**, 3110 - 3115 (2003).

[17] J. E. Clendenin and G. A. Mulhollan, SLAC-PUB-7760

[18] I. Ben-Zvi et al., “Ampere Average Current Photoinjector and Energy Recovery Linac”, Proc of FEL 2004.

[19] K. Floettman et al., :Emittance compensation in a superconducting rf gun with a magnetic mode”, Phys. Rev. ST-AB, **7**, 090702 (2004).

[20] L. Serafini, J. B. Rosenzweig, Phys. Rev. E **55** (1997) 7565.

[21] M. Ferrario et al., "HOMDYN study for the LCLS Photoinjector", in *The Physics of High Brightness Beams,* 534, World Scientific, 2000.

[22] M. Ferrario et al., Recent advances and novel ideas for high brightness electron beam production based on photo-injectors, ", in *The Physicsand Application of High Brightness electron Beams,* 45, World Scientific, 2003.

[23] Linac Coherent Light Source (LCLS) Conceptual Design Report, SLAC-R-593 (2002).

[24] J.B. Rosenzweig and E. Colby, "Charge and Wavelength Scaling of RF Photoinjector Designs", *Advanced Accelerator Concepts* p. 724 (AIP Conf. Proc. 335, 1995).

[25] J. Sekutowicz et al., Nb-Pb superconducting RF-gun, submitted to PRST-AB.

[26] M. Ferrario, INFN-LNF, J.B. Rosenzweig, G. Travish, J. Sekutowicz, W. D. Möller, “An ultra-high brightness, high duty factor, superconducting rf photoinjector” Proc. of EPAC 2004, Lucerne, Switzerland

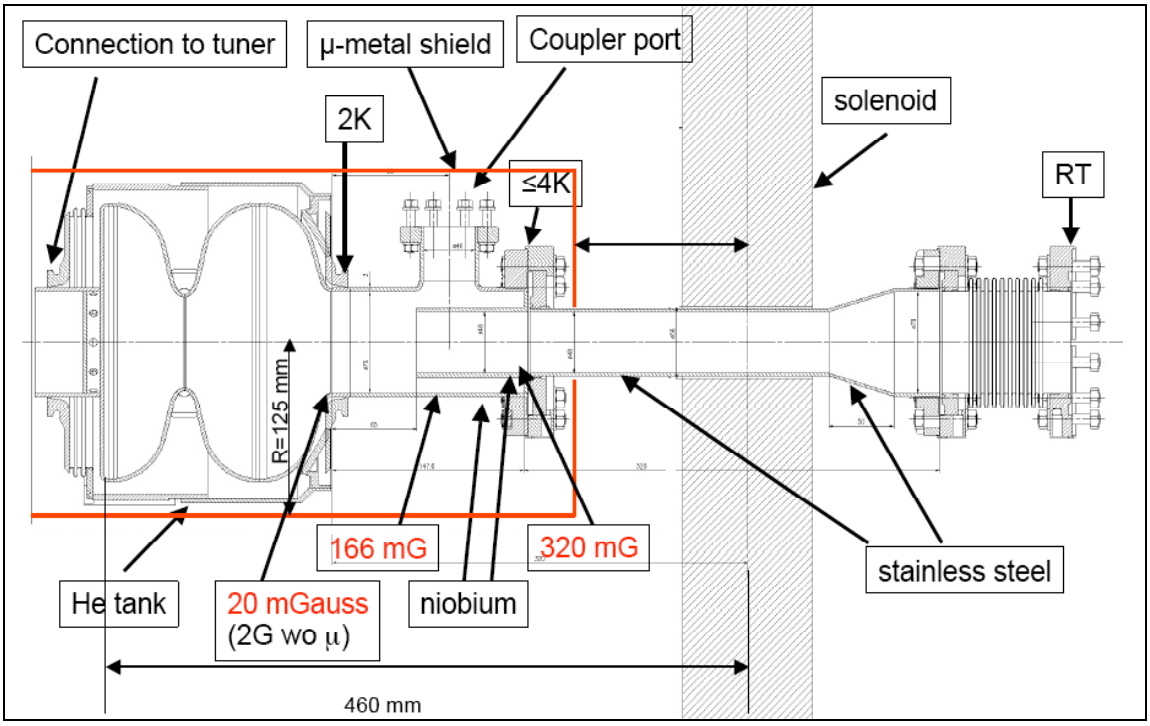
Connection to tuner
μ-metal shield
Coupler port
2K
≤4K
solenoid
RT
R=125 mm
166 mG
320 mG
stainless steel
He tank
20 mGauss
(2G wo μ)
niobium
460 mm

Figure 1

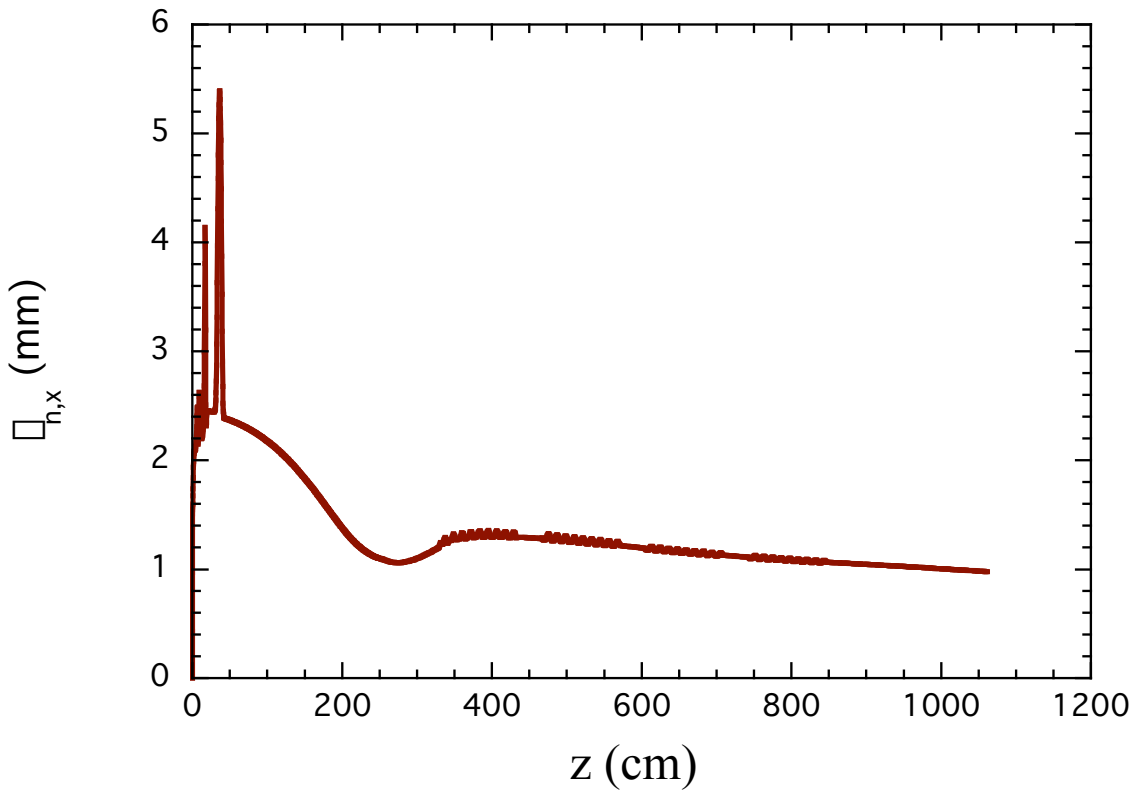

Figure 2

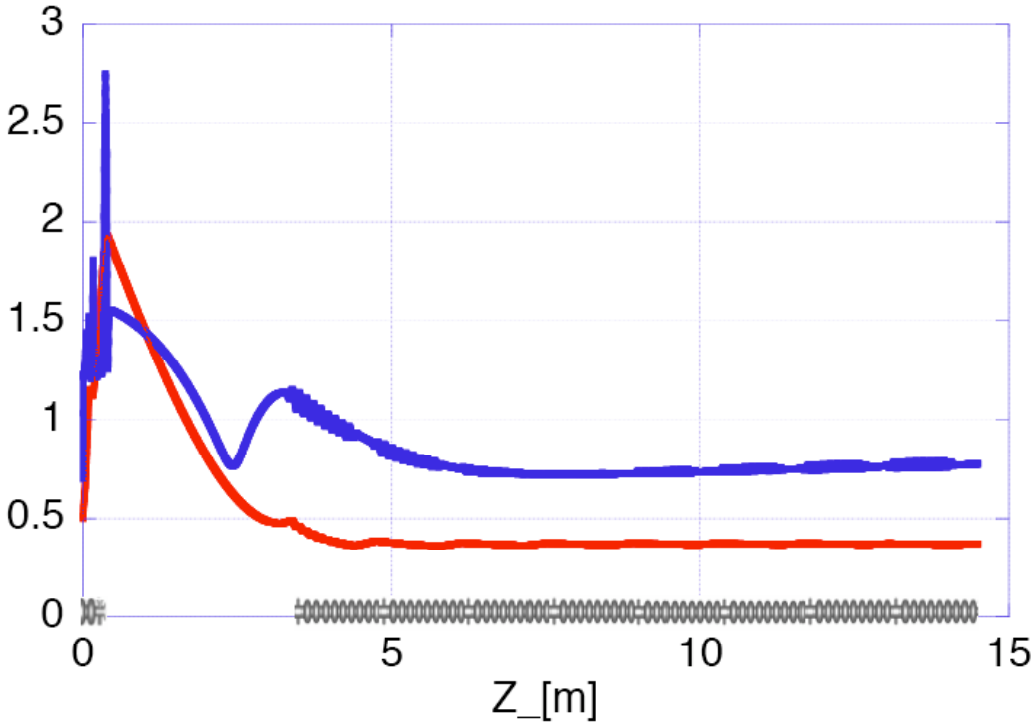

Figure 3

Emittance compensation with dynamically optimized photoelectron beam profiles

J. B. Rosenzweig, A.M. Cook, R.J. England, M. Dunning

UCLA Dept. of Physics and Astronomy

405 Hilgard Ave., Los Angeles, CA 90095, USA

S.G. Anderson

Lawrence Livermore National Laboratory

7000 East Avenue, Livermore, California 94550, USA

Massimo Ferrario

Istituto Nazionale di Fisica Nucleare, Laboratori Nazionale di Frascati

Via E. Fermi 41, Frascati (Roma), Italy

Corresponding author: J.B. Rosenzweig

UCLA Dept. of Physics and Astronomy

405 Hilgard Ave

Los Angeles, CA 90095, USA

Phone: 310-206-4541

FAX: 310-206-5251

e-mail: rosen@physics.ucla.edu

ABSTRACT

Much of the theory and experimentation concerning creation of a high-brightness electron beam from a photocathode, and then applying emittance compensation techniques, assumes that one must strive for a uniform density electron beam, having a cylindrical shape. On the

other hand, this shape has large nonlinearities in the space-charge field profiles near the beam's longitudinal extrema. These nonlinearities are known to produce both transverse and longitudinal emittance growth. On the other hand, it has recently been shown by Luiten that by illuminating the cathode with an ultra-short laser pulse of appropriate transverse profile, a uniform density, ellipsoidally shaped bunch is dynamically formed, which then has linear space-charge fields in all dimensions inside of the bunch. We study here this process, and its marriage to the standard emittance compensation scenario that is implemented in most recent photoinjectors. It is seen that the two processes are compatible, with simulations indicating a very high brightness beam can be obtained. The robustness of this scheme to systematic errors is examined. Prospects for experimental tests of this scheme are discussed.

PACS: 29.25.Bd, 29.25.Bx, 41.75.Ht

Keywords: Emittance, brightness, space-charge, collective effects, electron source

1. INTRODUCTION

In order to obtain the highest brightness electron beams from photoinjectors, it is most common to rely on the *emittance compensation* process[i]. Optimization of this process demands that the transverse fields be as uniform, and linear (in radius r) as possible. Most of the existing theoretical and experimental studies of emittance compensation have, to that end, assumed use of a uniform density electron beam, having a cylindrical shape. However, this shape produces space-charge fields near the beam head and tail that have pronounced nonlinear dependences on the spatial coordinates. These nonlinearities result in both transverse and longitudinal emittance growth.

It has been known for some time[ii], however, that a uniform density distribution having ellipsoidal shape yields space-charge fields that are linear in all dimensions (e.g. $E_x \mu x$, $E_z \mu z$). Under such conditions, it is conceivable that one may obtain essentially emittance-growth-free dynamics. How to produce such a distribution has, until recently, remained an unanswered question. Limborg has discussed schemes for manipulating and shaping the photoinjector drive laser pulse so that it has an ellipsoidal distribution[iii]. This scheme gives good results, as it is a refinement of the standard LCLS emittance compensation scenario[iv], with an improved beam distribution. On the other hand, implementation of this scheme has serious technical challenges.

In 1997, Serafini proposed the dynamic creation of an ellipsoidal bunch by launching an ultra-short, radially shaped beam[v], which then evolves through longitudinal expansion of differing radii in the beam to achieve the desired longitudinal shape. In this work, a 10's of femtosecond laser pulse with uniform time profile was assumed, which is not technically

feasible — pulses this short are now a routine capability of the photocathode drive lasers, but not with such a restrictive profile. On the other had, it has recently been shown by Luiten, *et al.,*[vi] that in obtaining the correct final ellipsoidal distribution, there is essentially no requirement on the shape of the initial laser pulse other than it be ultra-short (length Δ_l much shorter than eventual beam length after space charge expansion). Thus it is a natural, and technically achievable way of producing an ellipsoidal-shaped, nearly uniform density beam.

As the beam dynamics just after photoemission are qualitatively different in the traditional emittance compensatio scenario and in Luiten's scheme, it is not immediately apparent that one may successfully combine the two. We study here this possibility, showing that the marriage of emittance compensation and dynamic creation of the ellipsoidal shaped beam produces results that in many ways are superior to those obtained in state-of-the-art designs. As the bunches that are produced are shorter in such standard cases, very high brightness beam creation will be shown to be possible.

In this paper, we begin with a detailed examination of the longitudinal beam dynamics characteristic of ultra-short pulse operating regime. We then explore, using multiparticle simulations, the conditions under which one may obtain emittance compensation in existing photoinjector experimental setups. Deviations from ideal performance, both from physical effects in or near the cathode, and systematic errors, are discussed. Prospects for experimental tests of this scheme are examined.

2. LONGITUDINAL BEAM DYNAMICS

In the Serafini-Luiten scheme, the beam profile expands and deforms longitudinally to produce, in the final state, a uniformly filled ellipsoid of charge. In the process, phase space rearrangements occur which degrade the emittances — especially in the longitudinal dimension. In order to understand this process, to specify experimental requirements, and to identify experimental signatures associated with the process, we analyze in the following the dynamics of space-charge-dominated beam expansion. We note that the reconfiguring of charge to produce a uniform density is a ubiquitous process in single-component plasmas, of which beams are a prime example. Thus our analysis borrows methods and conceptual framework from previous work in the context of transverse space-charge[vii,viii,ix].

We begin by assuming illumination of a photocathode with a laser having a time profile given by the normalized (to unity) function $g(t_0)$, which produces emission up to a radius a. Assuming prompt electron emission, the photocurrent is

$$I(t_0) = Qg(t_0), \tag{1}$$

where Q is the total beam charge, and the emission time is characterized by $g_{\max} \sim \tau^{-1}$. We assume now that $c\tau << a$, so that the beam's electric field is predominantly longitudinal.

Ignoring the effects of the cathode image charge, we calculate the longitudinal force on an electron as

$$\begin{aligned} F_z(t_0) &= -eE_0 + 4\pi e\sigma_b(r)\int_0^{t_0} g(\tilde{t}_0)d\tilde{t}_0 \\ &= -eE_0 + 4\pi e\sigma_b(r)G(t_0) \\ &= -eE_0\left(1 - \Gamma(r)G(t_0)\right). \end{aligned} \tag{2}$$

Here we have defined the function $G(t_0) = \int_0^{t_0} g(\tilde{t}_0)d\tilde{t}_0$ as the integrated (from beam center), fractional beam charge. We have implicitly assumed that G is only a function of t_0, and can therefore be calculated once and for all at emission. This assumption, that electrons do not overtake each other, is termed *laminar flow*. It was assumed, but not shown to hold, in Refs. 5 and 6 that laminarity holds; here we shall illustrate that it indeed does so. The quantity $\sigma_b(r)$ is the beam surface charge density distribution in r. The maximum field associated with a surface charge is $4\pi\sigma_b$, and so we normalize the value of the space-charge field through $\Gamma(r) = 4\pi\sigma_b(r)/E_0$. Luiten, *et al.*, have given the condition $\Gamma << 1$ as a requirement for ignoring image charges; we assume that it is satisfied. As no significant transverse electric fields are present by assumption, we take r as constant.

Under these assumptions we can write the energy of a given electron as

$$\gamma(z,r,t_0) = 1 + \Gamma(r,t_0)z, \tag{3}$$

where

$$\Gamma(r,t_0) = \frac{F_z(r,t_0)}{m_e c^2} = \Gamma_0\left(1 - \Gamma(r)G(t_0)\right) \text{ and } \Gamma_0 = \frac{|eE_0|}{m_e c^2}. \tag{4}$$

Given the energy, one may find the velocity, and integrate it to find z as a function of t,

$$c\left[t(r,t_0) - t_0\right] = \int_0^z \frac{d\tilde{z}}{\gamma(\tilde{z},r,t_0)} = \frac{1}{\Gamma(r,t_0)}\int_1^{\gamma(z,r,t_0)} \frac{d\gamma}{\sqrt{\gamma^2 - 1}} = \frac{1}{\Gamma(r,t_0)}\sqrt{\left[\Gamma(r,t_0)z\right]^2 - 2\Gamma(r,t_0)z}. \tag{5}$$

After the electron is relativistic, the relative longitudinal motion slows to give an asymptotic form of the final time

$$c\left[t_f(r,t_0)\right] - z + ct_0 + \frac{1}{\Gamma(r,t_0)} - \frac{1}{\Gamma_0}. \tag{6}$$

Equation 6 may be used to deduce the form of the final beam distribution. Conservation of probability yields that the current expands by the factor $\partial t_0 / \partial t_f$, and so the final current density is given by

$$J\left(r,z,t_f\right) = \frac{g\left(t_0\right)\rho_b\left(r\right)}{\partial t_f / \partial t_0}, \tag{7}$$

where, under our assumptions, we may write

$$\frac{\partial t_f}{\partial t_0} = 1 + \frac{\gamma_0 \Phi\left(r\right)}{c\tau^2\left(t_0\right)} g\left(t_0\right) \approx 1 + \frac{\Phi\left(r\right)}{c\tau_0} g\left(t_0\right). \tag{8}$$

Note that "wave-breaking" or loss of laminarity [9] is given by the condition $\partial t_f / \partial t_0 = 0$, which is not allowed inside of the beam (g>0); the assumption of laminarity is validated. The current density deduced from Eqs. 7 and 8 is

$$J\left(r,z,t_f\right) = \frac{g\left(t_0\right)\Phi\left(r\right)}{1 + \frac{\Phi\left(r\right)}{c\tau_0} g\left(t_0\right)}, \tag{9}$$

which, assuming significant expansion ($\Phi\left(r\right) >> c\tau_0$), approaches a constant value,

$$J\left(r,z,t_f\right) \approx \frac{eE_0^2}{4\pi m_e c}. \tag{10}$$

We therefore deduce that the beam density is uniform, inside of certain boundaries. In order to calculate where the beam edges are, we follow the extrema in the longitudinal coordinate (dropping the constant z of the beam centroid),

$$\begin{aligned} c\left[t_f\left(t_{0,edge}\right)\right] &\approx ct_0 + \frac{1}{\Phi\left(r,t_{0,edge}\right)} \approx \frac{1}{\tau_0} \\ &\approx ct_0 + \frac{\Phi\left(r\right)}{2\tau_0} \approx \frac{2\pi m_e c^2}{E_0^2}\rho_b\left(r\right) \end{aligned}. \tag{11}$$

The position of the bunch boundary in t, and therefore in z, is thus proportional to $\rho_b\left(r\right)$. In order to have this boundary be an ellipse in (r,z) one chooses the surface charge density as

$$\rho_b\left(r\right) = \frac{3Q}{2\pi a^2}\left(1 - \left(\frac{r}{a}\right)^2\right)^{1/2}, \tag{12}$$

to obtain

$$ct_{f,edge} \approx \frac{3Qm_e c^2}{E_0^2 a^2}\left(1 - \left(\frac{r}{a}\right)^2\right)^{1/2}. \tag{13}$$

Several phenomena that do not occur in a standard geometry ($\square_b(r) = \text{constant}$) are apparent from this analysis. First, one has mixing of electrons between slices during the expansion. Because of this, there is an initial fast increase of the longitudinal emittance, which is terminated by the transition of the field direction from predominantly longitudinal to mainly transverse as the beam accelerates. This "missing" region of transverse space-charge also differentiates this scenario — the geometry of the injected beam in the standard configuration has a length much longer than the radius, and transverse space-charge forces assert themselves nearly immediately, within a propagation length approximately equal to the beam radius. In the Serafini-Luiten scheme, pulse length expansion is required, while in the standard scenario it is avoided.

The formalism we have presented above allows calculation of the transient increase in energy spread and longitudinal emittance during the longitudinal-field dominated region of beam propagation. It does not, however, indicate when the transition from longitudinal field domination to transverse occurs. Thus, even though one may predict the longitudinal expansion from our formalism, the continued growth of longitudinal phase space quantities, unaccompanied by significant expansion, cannot be calculated from Eqs. 3 and 4. Simulations must be used to explore these issues, along with the central issue of emittance compensation.

3. SIMULATIONS AND EMITTANCE COMPENSATION

We have performed initial UCLA PARMELA[x] simulations to explore the joining the Serafini-Luiten scheme with the optimized emittance compensation working point (pioneered or the LCLS), of the SPARC injector at LNF-Frascati. We assume that the gun (1.6 cell, 2856 MHz) and solenoid are the same, and run in near to the standard conditions. Through trials, we have optimized the launch conditions of the beam. In order to have values of $\square$ which do not give excessive image charge effects the beam charge is lowered, and the beam radius is slightly enlarged. In a preliminary optimization, we launch a 0.33 nC beam with an initial longitudinal Gaussian distribution having $\square_t$ =33 fs beam, and a radial Gaussian with $\square_x$ =0.77 mm (cutoff at 1.8 $\square$). The gun is run with peak, on-axis gradient of 120 MV/m, and the beam is launched at 33 degrees forward of crest. This is well forward of the nominal launch phase for a standard bunch, and serves to control the excessive beam energy spread after the gun. The emittance compensation solenoid is run with peak field B_z= 2700 G, which is slightly

below the standard scenario, as the beam has slightly lower energy exiting the gun. We note that the peak value of ρ in our case is 0.11, as opposed to 0.42 in the LCLS design.

There is of course an initial transverse growth emittance which occurs during the reconfiguration of the bunch charge near the cathode, and subsequent growth which may occur to the imperfections in the quasi-ellipsoidal distribution that is formed. It is these effects that are addressed by the emittance compensation process. Emittance compensation is accomplished in two steps: the focusing of the beam by the post-gun solenoid, and the matching of the beam in the first traveling wave linac section (3 m long, SLAC-type, 13.5 MV/m average acceleration), which has a 560 G solenoid field overlaid on it.

The formation of the quasi-ellipsoidal bunch is clearly shown in Fig. 1, which displays the bunch (x,z) distribution at a point 133 cm from the cathode, in the drift space after the gun and just preceding initial traveling wave linac section. Here the beam has 6.3 MeV mean energy, and its transverse dynamics are space-charge dominated. Thus one sees clearly the "inflated" ellipsoidal beam shape. As this shape is obtained purely through space-charge effects, the 6-dimensional transverse phase space is indeed close to the ideal Kapchinskii-Vladimirskii distribution [2]. The final bunch length is 1.3 mm full width, corresponding to a peak current of 117 A. Thus even with one-third of the charge, this scheme should produce a higher current than obtained in simulations of the standard design

Two notable defects are seen in the beam shape in Fig. 1. The first is the extension of the half-ellipsoid in the trailing part of the bunch as compared with the initial half. This asymmetry is caused by image charge effects. This non-ideal behavior in fact gives the limit on σ; when one attempts to launch a higher surface charge density, the bunch deformation from the desired symmetric ellipsoid produces poor emittance performance. The second notable feature is the existence of an anomalous ring at the outer radial edge of the beam. This part of the beam has low surface charge density and experiences radially fringing fields due to its edge location. Because of this, it does not experience enough longitudinal expansion to keep pace with the rest of the bunch, but instead has a moderate amount of radial expansion.

As the longitudinal space-charge during much of the acceleration is also linear, and total pulse length T is short, the longitudinal phase space is very compact. The evolution of the relative momentum spread $\sigma_{\delta p/p}$ in z is shown in Fig. 2. The final achieved rms value is $\sigma_{\delta p/p} = 1.6 \cdot 10^{-4}$, which is an order of magnitude smaller than that obtained in the standard LCLS-type design.

The evolution of the rms transverse beam size σ_x, and the rms normalized emittance $\varepsilon_{n,x}$ are shown in Figs. 3 and 4, respectively. While the behavior of σ_x is similar in most respects to the standard design, with the approximately beam matched at linac entrance to the invariant envelope [1,4], the emittance behavior is not as familiar. In the standard LCLS design, $\varepsilon_{n,x}$ achieves a minimum value in the post-gun drift, rising to a local maximum at injection into the linac. The focusing and adiabatic damping of the motion in the linac then produce a monotonic decrease of $\varepsilon_{n,x}$ in z. In our case, the transverse space-charge and thus the plasma/emittance oscillations [1] do not "turn on" until after the longitudinal expansion is well underway, thus delaying the emittance minimum in Fig. 4 to occur inside of the linac. In order to produce faster emittance oscillations in the linac to strongly diminish $\varepsilon_{n,x}$ before acceleration removes the plasma-dominated beam behavior, the solenoid field in the first linac section has been raised by 40% relative to the standard scenario. This ploy works well, as the final value (still slightly diminishing) of $\varepsilon_{n,x}$ at the end of the second linac (84.5 MeV energy) is 0.68 mm mrad. The thermal emittance at the cathode is 0.4 mm mrad, and so the space-charge induced emittance is well compensated.

After acceleration to higher energy (84.5 MeV), the beam is not space-charge dominated, and the (x,z) profile no longer ellipsoidal, as shown in Fig. 5. Nonetheless, the beam has excellent emittance, and maintains a current profile with shape $I \mu \sqrt{1-(2t/T)^2}$.

With a high initial current, and low intrinsic energy spread, this beam may be compressed further, with very high final peak current achievable. In Fig. 6, we show the resulting longitudinal phase space calculated by a further simulation, using Elegant[xi] (with input obtained from PARMELA output), of post-acceleration running forward of crest, and then encountering a chicane. The distribution shown has a final rms bunch length $\sigma_z = 11$ μm (σ_t = 37 fs), with a peak current of 4.5 kA. This beam, which has only 0.4% rms momentum spread, has obvious utility in ultra-short pulse FEL or inverse-Compton scattering experiments.

4. BRIGHTNESS LIMITS

As the compensation process produces an emittance close to that due to thermal effects at the cathode, the maximum brightness may be calculated for this scheme, which seems to be nearly optimum.

To start, we note that the brightness is given in the simulations case is

$$B_{\max} = \frac{2I}{\varepsilon_n^2} = 5 \times 10^{14} \text{ A/(m rad)}^2, \tag{14}$$

exceeding that of the LCLS design scheme by a small factor. Using the as the analysis above as a guide, one may in principle do even better, with

$$\begin{aligned} B_{\max} &= 8\pi J_{\max} \left(\frac{m_e c}{\varepsilon_{p,x}} \right)^2 \\ &\approx \frac{2eE_0^2 m_e c}{\varepsilon_{p,x}^2} \approx \frac{ecE_0^2}{k_b T_c}, \end{aligned} \tag{15}$$

where we have used Eq. 10, k_B is the Boltzmann constant, and T_c is the effective cathode temperature. Note the striking scaling that the brightness is now independent of the charge in this regime. For a Mg cathode under illumination by a frequency-tripled Ti:Sapphire laser under the electric fields assumed, $k_B T \approx 0.9$ eV, the maximum brightness is deduced to be $B_{\max} \approx 3.75 \times 10^{15}$ A/(m - rad)^2. This is a factor of 7.5 larger than achieved in the simulations, because: (1) the maximum brightness refers only to the central slice, and so the projected emittance calculated in the simulation provides an over-estimate in the context of Eqns. 14 and 15, (2) the emittance does not reach the thermal limit, and (3) additional pulse lengthening occurs after the gun which is not accounted for in the theoretical analysis. All of these effects may be mitigated, and one may expect to approach the optimum brightness with further refinements of the scheme.

4. EXPERIMENTAL OUTLOOK

Several experimental scenarios are now under investigation, including the PLEIADES injector at LLNL[xii], the SPARC injector, and the ORION injector at SLAC[xiii]. All have the approximately the same gun design (each fabricated at UCLA), and all have traveling wave post acceleration linacs with solenoid focusing overlaid. All of these injectors possess lasers with 100 fs pulse capability, and are adequate for studying the physics of this regime. The PLEIADES injector is not laid out according to the Ferrario optimization, however, and has a non-standard emittance compensation solenoid, as well as a short gun-linac drift distance. The ORION injector is nearly identical to the case studied here, but employs higher gradient X-band linac sections. The SPARC injector is, of course the example we have employed here, and is thus ideal for exploring the physics we have discussed above. This collaboration is now weighing the relative merits of each site.

The experimental signatures that one looks for in tests of this photoinjector operating regime may be delineated. In general terms, the complete emittance compensation scenario presented will show good emittance performance, along with a higher current and short pulse. In addition, at low energy, the beam will have an ellipsoidal shape. This shape may be viewed trivially in z-projection by a standard profile monitor (scintillating crystal, optical transition radiator, etc.). In terms of the longitudinal profile, one may consider use of a streak camera, with an aerogel Cerenkov radiator, to observe the time dependence of the current, and spatially resolve the transverse direction, thus measuring for example, a (x,z) slice of the beam, which should give a uniformly filled ellipse. By scanning this slice in x position, one may reconstruct the entire ellipsoid. Streak cameras may have time resolution as low as 0.25 ps (in practice it may be a bit larger), which is adequate to resolve our beam, which is longer than 4 ps full width. The z-projected transverse phase space (in one dimension) may be investigated at low energy using the multi-slit technique[xiv].

At higher energy, one may observe the final state of well-compensated emittance through quadrupole scanning[xv] or transverse phase space tomography[xvi]. The ellipsoidal beam in not observable at this energy, as the beam transverse distribution is emittance, and not space-charge dominated, as shown in Fig. 5. The longitudinal distribution can be time-resolved at higher energy at the SPARC injector[xvii] using a fast RF sweeper[xviii] with around 30 fs resolution. One may also use longitudinal phase space tomography to observe the higher quality longitudinal phase space. In addition, at SPARC one may use a downstream compressor to investigate compression to the ultra-short bunch length illustrated in Fig. 6. This bunch length presents challenges in measurement, stressing both coherent radiation techniques[xix], and RF deflectors.

5. DISCUSSION AND CONCLUSIONS

We have analyzed the feasibility of the marriage between the Serafini-Luiten dynamic beam expansion that produces uniform, ellipsoidally-shaped distribution and standard emittance compensation. With some small modifications, it has been seen that they are compatible, and that very high brightness beam performance is obtained in this new scenario. The positive aspects of this proposed operating regime are many. In this scheme, the transverse emittance is found to be quite good, and the longitudinal phase space much improved. One aspect of the quality of the longitudinal phase space is higher current (shorter pulse); another is lower energy spread. Further, the current profile in this regime gives a much improved form of longitudinal wake-fields in addition to the noted improvement in linearity of space-charge forces. These improvements

combine to produce a notable improvement in the pulse compression process, mitigating the tendency to produce spikes in the compressed current profile.

Technically, it should noted that the demands on the longitudinal laser pulse-shaping are minimized in comparison with the more standard “beer-can” shape previously assumed. The needed pulse widths can be obtained from many of the existing photoinjector drive lasers, which are designed with large bandwidth (short pulse capability) to allow pulse shaping of the flat-top profile with fast rise-small times. Likewise, the transverse pulse shaping is not any more challenging than in the standard case.

Foreseeable drawbacks of this scheme include the limitations imposed by cathode image charges, and large energy spread which is present during the compensation process (*cf.* Fig. 2). These are design considerations, however, and apparently do not introduce strong constraints on performance. The scheme is, on the other hand, much more dependent on laser fluctuations. Overall laser energy changes directly introduce systematic pulse length variations. Illumination or quantum efficiency non-uniformities will also cause notable degradation in the emittance compensation process in this regime. Perhaps the most serious question in implementing this scheme is the promptness of the photoemission — metals should give fast enough response (a few 100 fs is adequate), but high quantum efficiency semiconductor cathodes are probably not. On a similar note, one may need to be concerned with the peak laser intensity that is demanded on the cathode in this scenario, and choose a laser

In all, the outlook for implementation of this scheme is quite positive. Direct experimental tests of the relevant physics and technology are expected within the next year, allowing a more definitive judgment on the usefulness of this regime in time for deployment on the high brightness beam injectors for FELs and other light sources.

ACKNOWLEDGEMENTS

The authors would like to thank Luca Serafini for useful discussions over many years on this subject. This work was performed under the auspices of the U.S. Department of Energy under contract numbers DE-FG-98ER45693 and DE-FG03-92ER40693.

FIGURE CAPTIONS

Figure 1. PARMELA simulation results, showing electron bunch (x,z) distribution 133 cm from cathode (6.3 MeV energy), before injection into the first linac section, showing ellipsoidal beam boundary.

Figure 2. Evolution of $\sigma_{\Delta p/p}$ in z for emittance compensation case, from PARMELA simulation.

Figure 3. The evolution of rms transverse beam size σ_x for emittance compensation case, from PARMELA simulation.

Figure 4. Evolution of rms normalized emittance $\varepsilon_{n,x}$ for emittance compensation case, from PARMELA simulation.

Figure 5. Electron bunch (x,z) distribution after second linac section (84.5 MeV energy), with ellipsoidal beam shape no longer apparent, from PARMELA simulation.

Figure 6. Longitudinal phase space after third (off-crest) linac section and chicane, showing compression of pulse to σ_z =11 μm, from Elegant/PARMELA simulation.

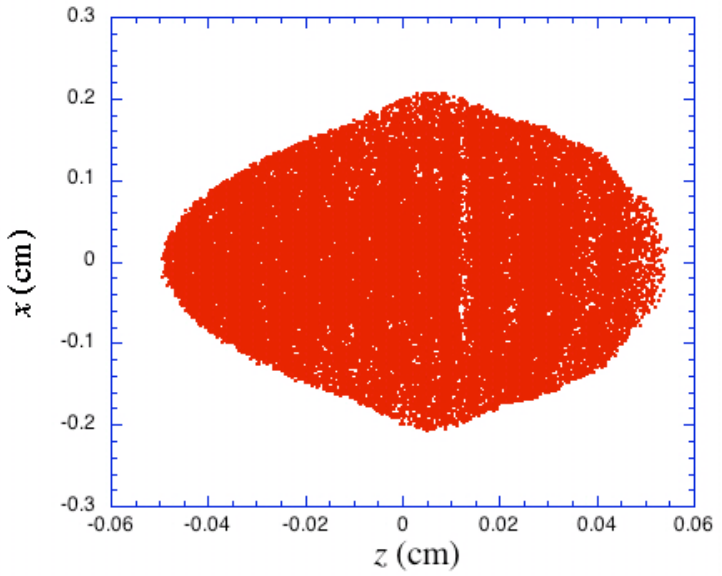

Figure 1

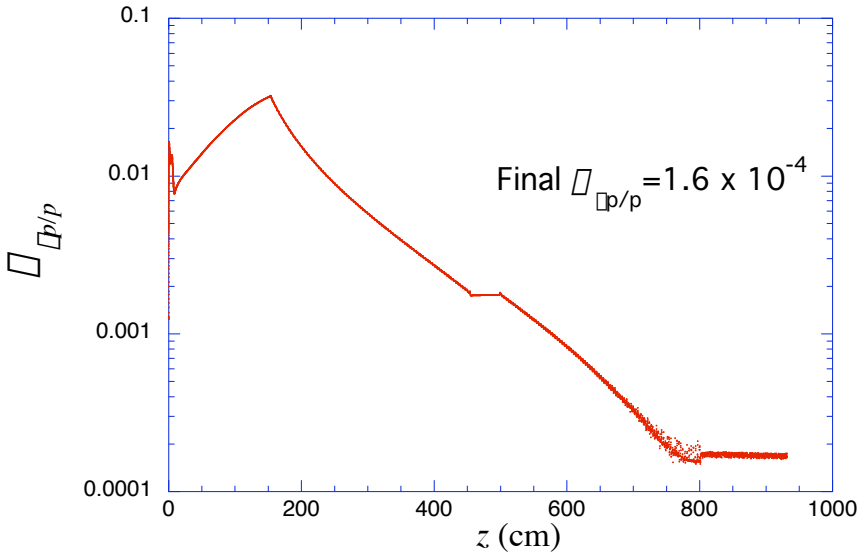

Figure 2

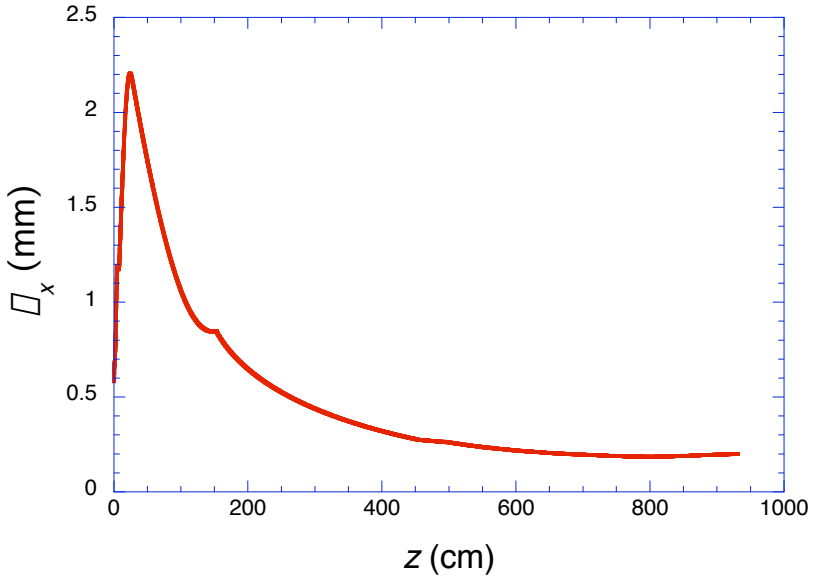

Figure 3

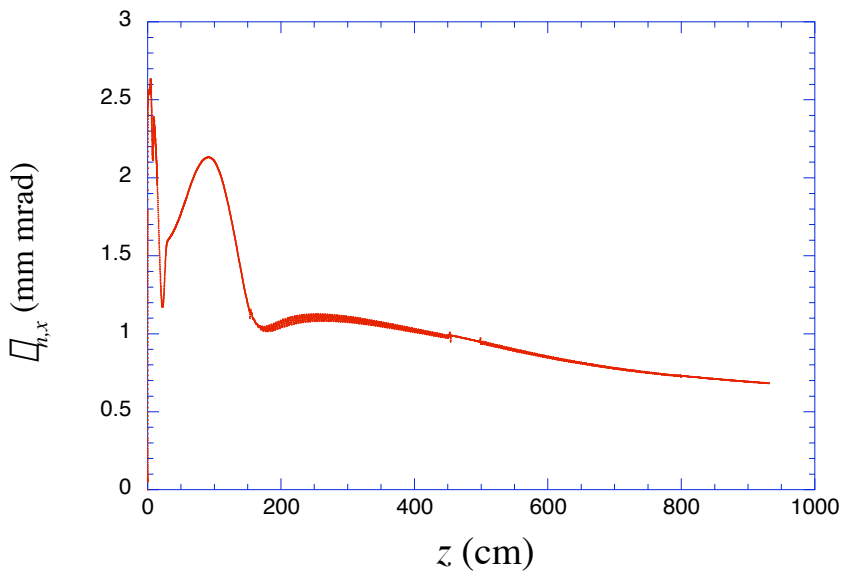

Figure 4

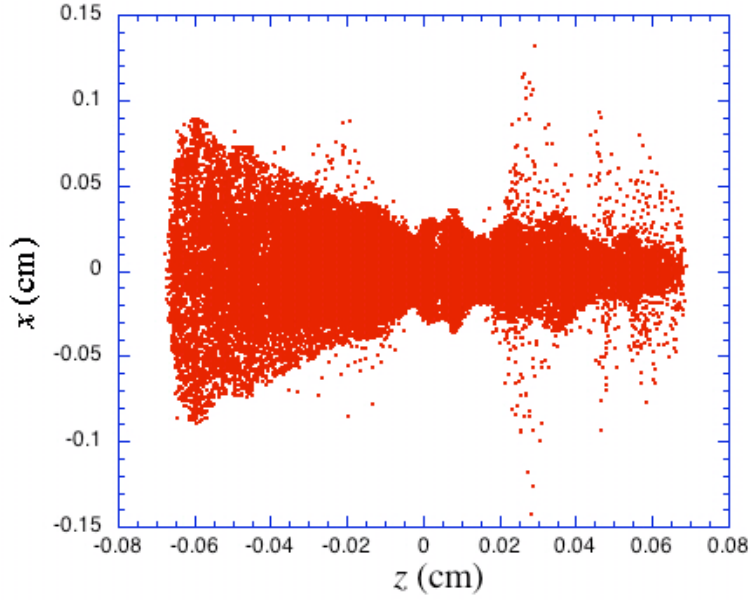

Figure 5

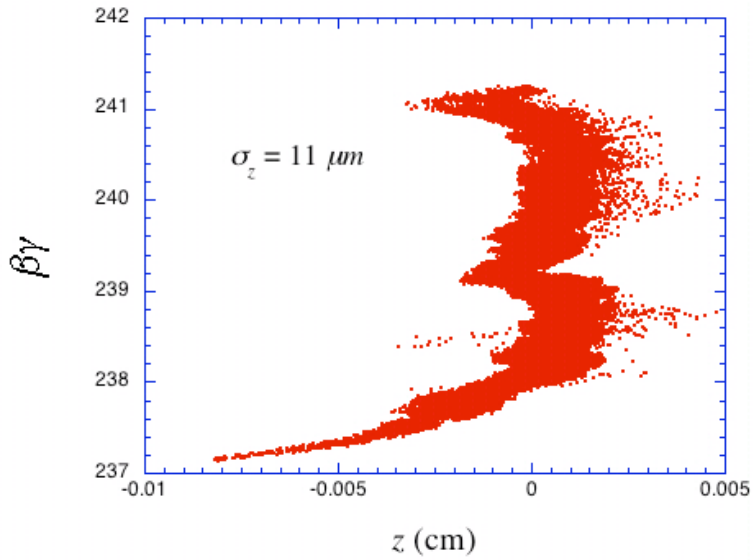

Figure 6

REFERENCES

[i]. Luca Serafini and J.B. Rosenzweig *Physical Review E* **55**, 7565 (1997).
[ii]. I.M. Kapchinskii and V.V. Vladimirskii, in *Proceedings of the International Conference on High Energy Accelerators*, CERN, Geneva (Scientific Information Service CERN, Geneva, 1959), p. 274.
[iii]. C. Limborg, these proceedings.
[iv]. M. Ferrario, J.E. Clendenin, D.T. Palmer, J.Rosenzweig, and L. Serafini, in *The Physics of High Brightness Beams,* 534 (Eds. J. Rosenzweig, L. Serafini, World Sci., 2000).
[v]. L. Serafini, AIP Conf. Proc. **413**, 321 (1997).
[vi]. O. J. Luiten, S. B. van der Geer, M. J. de Loos, F. B. Kiewiet, M. J. van der Wiel, *Phys. Rev. Lett.,* **93**, 094802-1 (2004).
[vii]. O. A. Anderson, Part. Accel. **21**, 197 (1987)
[viii]. I. Hoffman and J. Struckmeier, *Part. Accel.*, **21**, 69 (1987).
[ix]. S.G. Anderson and J.B. Rosenzweig, *Phys. Rev. ST – Accel. Beams* **3**, 094201 (2000).
[x]. E. Colby, UCLA PhD Thesis, FERMILAB-THESIS-1997-03 (FNAL, 1997)
[xi]. M. Borland, computer code ELEGANT, ANL, http://www.aps.anl.gov/asd/oag/oaghome.shtml.
[xii]. S. G. Anderson, P. Musumeci, J. B. Rosenzweig, W. J. Brown, R. J. England, M. Ferrario, J. S. Jacob, M. C. Thompson, G. Travish, A. M. Tremaine, and R. Yoder, Phys. Rev. ST – Accel. Beams 8, 014401 (2005).
[xiii]. D.T. Palmer, et al, Proc. 2001 Particle Accelerator Conf. 2251 (IEEE, 2001).
[xiv]. S.G. Anderson, J.B. Rosenzweig, G. P. Le Sage, J.K. Crane, *Phys. Rev. ST Accel Beams* 4, 014201 (2001).
[xv]. X. Qiu et al., Phys. Rev. Lett. 76, 3723 (1996).
[xvi]. V.Yakimenko, et al *Phys. Rev. ST Accel Beams*, 122801 (2003).
[xvii]. D. Alesini et al., *Nucl. Instr. Methods A* 528 (2004) 586.
[xviii]. X.J. Wang, Proc. 1999 Part. Accel. Conf. 229 (IEEE, 1999).
[xix]. A. Murokh, et al., Nucl. Instr. Methods A 410, 549 (1998).